Progress In Electromagnetics Research B, Vol. 87, 39–60, 2020

On the Design and Fabrication of Chained-Function Waveguide Filters with Reduced Fabrication Sensitivity Using CNC and DMLS

Yuan Ping Lim, Sovuthy Cheab*, Socheatra Soeung, and Peng Wen Wong

Abstract—In this paper, we present the design and fabrication of a novel class of emerging waveguide filters based on chained-functions at the millimeter-wave band. The derivation of chained-functions by chaining of prescribed generalized Chebyshev seed functions based on the partition theory is presented in details, and the implementation to waveguide technology is proposed and evaluated. The waveguide filter is fabricated through two different technologies, namely the Computer Numerical Control (CNC) milling technology and the Direct Metal Laser Sintering (DMLS) based additive manufacturing technology. The chained-function filters, which lie in between the Butterworth and Chebyshev filters, inherit the salient properties of both Butterworth and Chebyshev filters. Therefore, the chained-function waveguide filter exhibits filtering responses that have a superior rejection property and a lower loss with reduced sensitivity to fabrication tolerance than the standard Chebyshev waveguide filter. The efficiency of the proposed waveguide filter is confirmed both theoretically and empirically, using the CNC and DMLS processes. The issues of a higher manufacturing tolerance and apparent surface roughness associated with the DMLS method are found to be electrically insignificant when the chained-function concept is adopted in waveguide filter design. In general, the measured results of all the realized waveguide filters agree well to those of the simulation models. These results positively demonstrate that the chained-function concept has robust properties for rapid, high-performance, low-cost, and sustainable filter design and implementation, particularly for higher millimeter-wave frequency bands and for narrow-band applications.

1. INTRODUCTION

The past decade has witnessed a rapid growth and revolution of wireless communication systems, with many new research ideas and product innovation currently in the pipeline. The inundation of mobile communication leads to congestion of the current allocated radio frequency (RF) spectrum and upsets the existing microwave filter technology. The RF spectrum has to be pushed to higher millimeter-wave bands for obtaining a higher channel capacity to accommodate the increase in mobile traffic. This impending technology will impact the current filter design technologies, prompting to the development of new filters to support and sustain the millimeter-wave communication. As such, the need pertaining to extreme filter specifications for channel filters must be readily available in order to optimize the spectrum utilization and to avoid spectrum interface. In contrast to the conventional filters, millimeter-wave filters operate at a higher frequency band. Hence, the filters will be highly sensitive to component value variations. Furthermore, at these frequency bands, the filters often suffer from high passband insertion loss; therefore, manufacturers often need to be extra careful in the fabrication process. This, in turn, results in complex and expensive manufacturing processes.

Received 11 January 2020, Accepted 2 April 2020, Scheduled 8 April 2020
* Corresponding author: Sovuthy Cheab (sovuthy.cheab@utp.edu.my).
The authors are with the Electrical and Electronic Engineering Department, Universiti Teknologi PETRONAS, Bandar Seri Iskandar, Perak 32610, Malaysia.

In filter design, Chebyshev filters are the most common filter among other filter classes, as it possesses high rejection properties and equiripple passband response, with a given filter order [1–4]. For a Chebyshev response filter, however, once the suitable characteristics polynomial which meets the target filter specifications has been identified, the filter requires a minimum tolerance to component value variations and a specific unloaded-Q factor for each resonator. It should be noted that a small amount of variation to the filter design parameter will result in the deviation of the filter's target response, especially at the higher millimeter-wave frequency bands. Thus, a complex, time-consuming, and/or expensive post manufacturing tuning process is often required to compensate the fabrication tolerance. As a result, the design techniques of Chebyshev response filters have always been challenging.

It is well known that the filter design procedure always starts with the initial approximation stage by selecting a suitable transfer function which will meet the filter design target specifications. In [1–4], the limitations of the Chebyshev response filter reported therein can be solved at the beginning of the filter design stage, i.e., the initial approximation stage, by employing a completely new class of transfer function, known as the chained-functions. The chained-functions, on the other hand, can be found as a trade-off between the Butterworth and Chebyshev approximations, as it could transverse the good properties between both Butterworth functions (i.e., lower sensitivity, lower resonator unloaded-Q factor and lower filter losses) and Chebyshev functions (i.e., higher selectivity and higher out-of-band rejection) [1–4]. Therefore, the chained transfer functions concept can reduce, or even eliminate, the lengthy and complex manufacturing processes, and most significantly, the post manufacturing tuning processes. It is able to extend the state-of-the-art development in high-performance tuning-less filter to higher frequency of operation and narrow bandwidth applications.

1.1. Scope, Motivations and Aims

Even though the theory of chained-function filters is available in the current literature [1–4], it is still not clear how to synthesize and implement a chained-function in filter design. Therefore, the motivation of this research is to implement a chained-function to waveguide technology at the millimeter-wave frequency band. This is mainly because the waveguide technology can be exploited as an ideal candidate to operate at the higher millimeter-wave frequency band, due to its inherent high Q factor, low passband insertion loss, and high power-handling capability [5]. Next, a modern filter synthesis approach, i.e., the coupling matrix synthesis and matrix rotation technique is employed to model and reconfigure the lowpass prototype filter network. In [6–9], the stated coupling matrix synthesis and matrix rotation techniques can be used as an universal method in the design of high performance microwave filters. The coupling matrix synthesis and matrix rotation approach can be easily utilized once the characteristic polynomials of the filter have been identified. It is worth mentioning that one can also use reflection matrices for the similarity transformations to achieve the desired topology [10, 11].

Traditionally, waveguide filters or other microwave components are usually manufactured through a high-precision Computer Numerical Control (CNC) milling process. It is well known that this technology has been advancing for the past few decades, and waveguide components manufactured through the CNC milling process, which exhibits excellent measured results, have also been widely demonstrated in the current literature (e.g., [12–15]). However, as the RF spectrum continues to increase, the waveguide filters or other microwave components become smaller in feature size. This leads to an increasing demand for hardware miniaturization. Due to the small hardware feature, the CNC milling process often fails. This is because of the limitations with regard to the available cutter sizes, wear or breakage of cutters, generation of defects and cracks due to mechanical stresses [16]. Furthermore, extremely tight tolerances may need to be applied, and tuning elements often cannot be used when dealing with hardware miniaturization. This situation has created an unprecedented impact and challenges to the filter designers to return the filter's responses to its original target specifications. As a result, the relative development time and production cost of a filter increase dramatically.

An alternative solution to address the limitations of the CNC milling technology is the use of modern additive manufacturing technology (3D printing) in the filter fabrication process. Additive manufacturing technology can provide the state-of-art solution in terms of eliminating the use of cutters in the fabrication process; therefore, fabrication of high geometrical complexity structures is possible. In addition, the components manufactured by the additive manufacturing technology are free from integration, as they are typically printed as a whole piece. This means that this technology is more

robust and sustainable, as the final prototype utilizes less materials and volume than those from the CNC machining technology. As a result, additive manufacturing technology draws full advantages in terms of rapid prototyping and reduction in production cost and lead time.

Despite the aforementioned advantages, additive manufacturing technology possesses a lower resolution than that of the CNC milling technology, resulting in poor surface roughness and high manufacturing tolerances. In this paper, these drawbacks of the additive manufacturing technology can be compensated by the implementation of the novel chained-function concept in filter design. Due to the advantage of reduced sensitivity to manufacturing tolerances, the chained-function filters can be fabricated through the relatively low-cost additive manufacturing (3D printing) techniques with lower resolution without scarifying the filer performance. The feasibility of the chained-function concept in high frequency bands filter design can provide an unprecedented advancement towards rapid, high-performance yet cost-effective and sustainable filter design to revolutionize the filter design industry. Indeed, the chained-function filters contribute toward frontier research in millimeter-wave applications and support the usage of Internet-of-Things (IoT) and big-data based platforms for future 5G communication systems and beyond.

1.2. Contributions

The main contributions of this paper are summarized as follows:

1. We study the design, synthesis, and development of a novel state-of-the-art waveguide filter based on the chained-function concept and partition theory, using the coupling matrix synthesis approach, at millimeter-wave band. The waveguide filter has the property of reduced fabrication sensitivity to manufacturing tolerances.
2. We investigate the fabrication of the chained-function waveguide filter using two different manufacturing technologies; namely the conventional CNC milling based subtractive manufacturing technology and the modern DMLS based additive manufacturing technology. Both the manufacturing processes are investigated and compared.
3. We analyze and evaluate the measured performance from both the CNC and DMLS fabricated waveguide filters to identify the feasibility and potential fabrication technologies for millimeter-wave components.

1.3. Outline

The remaining part of this paper is organized as follows. In Section 2, the formulation of the chained-transfer-function based on the partition theory is described in details. In addition, the comparison of the chained-transfer functions with the standard Chebyshev and Butterworth approximation are outlined. In Section 3, the properties and performance of the chained function filters are investigated and compared with those of the conventional Chebyshev filters. The design and synthesis of the chained-function waveguide filter using the coupling matrix synthesis approach are presented in Section 4. Then, a working simulation pertaining to the chained-function waveguide filter is constructed using the ***ANSYS High Frequency Structure Simulator (HFSS)*** software to validate the filter design. In Section 5, we compare the fabrication of the filter by using the subtractive manufacturing (CNC milling) and additive manufacturing (DMLS) processes. The detailed description of both fabrication procedures are explained. The measurement results pertaining to the CNC and DMLS fabricated waveguide filters are detailed in Section 6, while the conclusions and recommendations for future work are presented in Section 7.

2. THE CHAINED TRANSFER FUNCTIONS

Transfer function is a mathematical function relating the output or response of a filter circuit to the input. It describes the characteristic and behaviour of a particular filter circuit. It is well known that the design and synthesis of a filter using the Butterworth approximation have the property of reduced sensitivity to filter parameter variations. It also requires a lower resonator unloaded-Q and exhibits a lower filter loss than the filter synthesized using Chebyshev approximation of the same order [2].

However, the out-of-band rejection performance and selectivity of the Butterworth response filter are worse than those of the standard Chebyshev response filter. In order to match the out-of-band rejection levels and selectivity with the standard Chebyshev response filter, the Butterworth response filter order needs to be significantly increased [2]. This, in turn, increases the filter complexity, thus, increases the production time and cost.

As mentioned in the introduction section, the Chebyshev response filter is still the most common filter among filter classes. The Chebyshev response filter is optimum in the sense that it can provide a very sharp rejection slope response with the lowest filter complexity. It should be noted that no other filtering functions exhibit these optimum characteristics. Due to the aforementioned reasons, even though the design and synthesis of a Chebyshev response filter do not have the mathematical simplicity as compared with that of the Butterworth response filter, it is still the preferable filter class for many filter designers.

The chained transfer functions, on the other hand, can be formulated by chaining of prescribed lower order generalized Chebyshev polynomials, known as the seed functions. For a given chained-function filter order of n_T, the partition theory is used to compute the number of possible seed-function combinations, SFC(n_T), as follows [1–4]:

$$\mathrm{SFC}\left(n_T\right) = P\left(n_T\right) \tag{1}$$

where $P(n_T)$ is the partition function. It should be pointed out that even though only the lower order generalized Chebyshev polynomials is considered as the seed functions in this paper, the theory is not restrictive in using other seed functions, subject to the application and provided that they are realizable. As an example, elliptic polynomials, Bessel polynomials, and Legendre polynomials can also be exploited as the seed functions. The total number of unrestricted seed function combinations for various filter order of n_T is summarized in Table 1.

Table 1. Number of unrestricted combinations for a filter order of n_T.

Filter Order, $\mathbf{n_T}$	**Partition Function $\mathbf{P(n_T)}$**
2	2
3	3
4	5
5	7
6	11
7	15
8	22

As an example, there are 5 different ways of partitioning a fourth order chained transfer function, i.e., $P(4) = 5$, while there are 7 different ways of partitioning a fifth order chained transfer function, i.e., $P(5) = 7$. Hence, it can be observed that a variety of novel chained transfer functions can be formulated for the same filter order after the chaining process. These transfer functions exhibit the same order but with different frequency-domains, time-domains, and implementation characteristics. The filter can be chosen to have the desired properties to suit the manufacturing limitations and different applications by selecting an appropriate seed function combination, i.e., reduction in sensitivity to parameter variations, lower resonator unloaded-Q requirements, and lower filter losses [1–4].

Table 2 shows the resulting chained transfer function for $n_T = 4$. It can be observed that a fourth order chained transfer function can be formed by chaining a third order with a first order Chebyshev approximation (i.e., $3+1$), or alternately, by chaining a pair of second order Chebyshev approximations (i.e., $2+2$), etc. The first row in Table 2 represents the Butterworth approximation, while the last row represents the Chebyshev approximation of the fourth order.

Notice that the chained-function concept with different seed function combinations allows a filter design with different out-of-band rejection performances and sensitivities, ranging from those associated with Butterworth to pseudo-Chebyshev and to Chebyshev. As an example, by partitioning n_T into the

Table 2. Seed function combinations and chained-function polynomials for a filter order of $n_T = 4$.

No. of Seed Functions	Seed Function Orders	Chained-Function Polynomials
4	$\{1, 1, 1, 1\}$	ω^4
3	$\{1, 1, 2\}$	$2\omega^4 - \omega^2$
2	$\{2, 2\}$	$4\omega^4 - 4\omega^2 + 1$
2	$\{3, 1\}$	$4\omega^4 - 3\omega^2$
1	$\{4\}$	$8\omega^4 - 8\omega^2 + 1$

first-order seed functions (i.e., $n_T = 1 + 1 + ... + 1$), a Butterworth filter response can be obtained. Similarly, by partitioning two or more lower-order seed function combinations, a pseudo-Chebyshev filter response can be obtained. The total filter order is given by the sum of the constituent seed function degrees.

3. THE CHAINED FUNCTION FILTERS PROPERTIES

There are many characteristics to determine a filter's performance. Among the most common ones are the out-of-band rejection performance, return loss performance, and filter sensitivity. These characteristics can be compared in a normalized lowpass prototype response. They can also be compared by using an appropriate frequency transformation technique and transforming them to the desired lowpass, highpass, bandpss, bandstop filter designs. In this section, we perform a performance comparison of the standard Chebyshev response filters with the novel chained response filters.

3.1. Out-of-Band Rejection Properties

When comparing the chained-function filters with the standard Chebyshev response filters, the out-of-band rejection properties of chained-function filters are slightly lower than those from the standard Chebyshev response filters [1, 2, 4]. This is because the optimum characteristics of the Chebyshev polynomial are distorted after the chaining process. For a Nth order chained response filter, there are no seed function combinations that can provide the similar (or better) out-of-band rejection properties, as compared with those of the standard Nth Chebyshev response filter. In other words, the selectivity and rejection properties of a chained-function filter will always be compromised.

Figures 1 and 2 are illustrative examples of the aforementioned phenomenon. The filters in the examples are designed for a return loss level of -25 dB using a passband ripple factor $\varepsilon \approx 0.0563$.

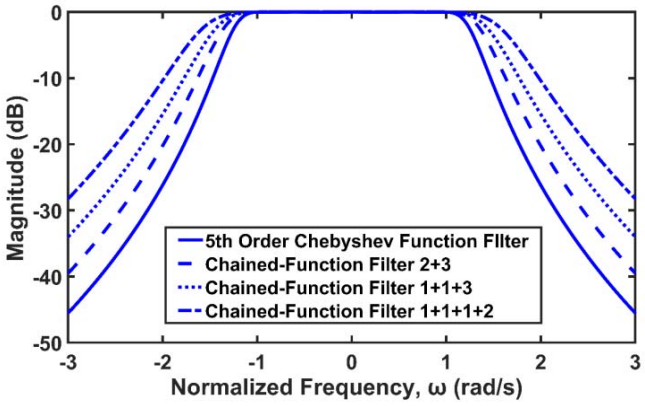

Figure 1. The out-of-band rejection slope for a 5th order Chebyshev function filter with various 5th order chained-function filters.

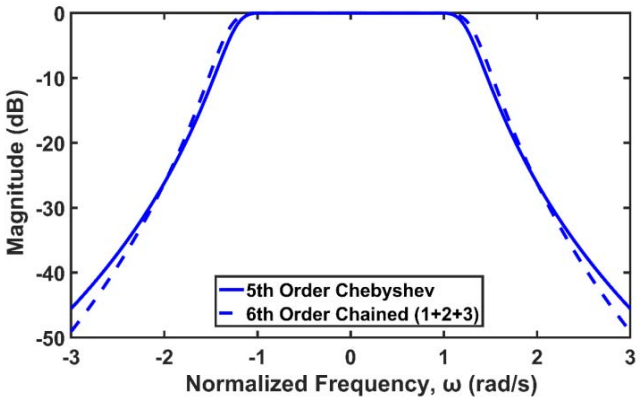

Figure 2. The out-of-band rejection slope for a 5th order Chebyshev function filter with a 6th order chained-function filter of order (1, 2, 3).

As can be seen in Fig. 1, for a 5th order chained-function filter, by any means, there are no seed function combinations to provide the equal out-of-band rejection properties as compared with those of the standard 5th order Chebyshev response filter. It can be observed in Fig. 2 that the out-of-band rejection properties of a 5th order standard Chebyshev response filter can only be achieved by a 6th order chained-function filter of order $(1+2+3)$, without any loss penalty. Therefore, it is clearly shown that the chained-function filter order needs to be slightly increased, in order to achieve similar (or better) out-of-band rejection properties corresponding to those of the standard Chebyshev type filter. In this respect, it is sufficient to increase the chained-function filter order by one.

3.2. Reflection Zeros Distributions

In particular, a critical factor in achieving the reduction in sensitivity or first pass tuning-less filter is by controlling the relative frequency separation of reflection zeros, which are distributed within the passband. It is well known that the wider the relative frequency separation of reflection zeros is, the lower the sensitivity of the filter is to parameter variation [1–4]. When designing a higher order narrow-band filter (e.g., a 6th order filter or higher), the relative frequency separation of reflection zeros becomes extremely small. Therefore, the filter will be extremely sensitive to parameter variations. Fig. 3 shows the distributions of reflection zeros for the 6th order Chebyshev response filter with various 6th order chained-function filters. All the filters are designed to achieve a return loss level of 25 dB.

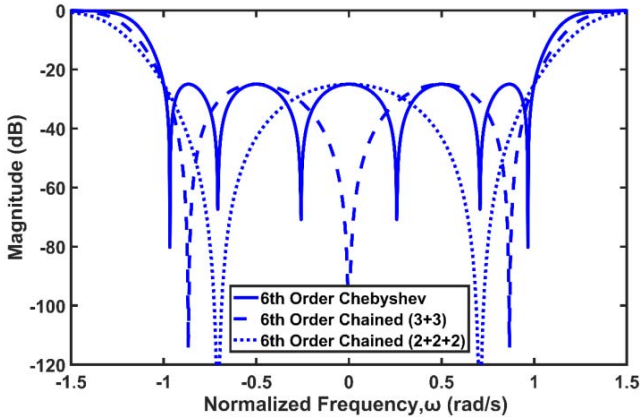

Figure 3. The distributions of reflection zeros for the 6th order Chebyshev response filter and various 6th order chained-function filters.

It should be noticed that for the chained-function filters, the reflection zeros are not equally distributed within the entire passband. In addition, the relative frequency separation of the reflection zeroes of the chained-functions filters is wider than those of the standard Chebyshev response filter. Theoretically, it means that the sensitivity of the chained-function filter is lower than those of the Chebyshev response filter, given the same filter order. Therefore, a filter designer can alter the filter sensitivity by modifying the position of reflection zeros.

3.3. Tolerance Effect and Sensitivity Analysis

A theoretical analysis is performed to prove that the sensitivity of a chained-function filter is lower than those of the standard Chebyshev response filters. Consider a 6th order chained-function filter of order $(1 + 2 + 3)$, a 6th order Chebyshev response filter, and a 5th order Chebyshev response filter. All these three filters are designed to achieve the same return loss performance of 21.14 dB, and their corresponding coupling matrices are synthesized. Equations (2), (3), and (4) show the coupling matrices of the 6th order chained-function, a 6th order Chebyshev response, and a 5th order Chebyshev response filter, respectively. The theoretical lowpass prototype responses of all the three filters resulting from their corresponding coupling matrices are depicted in Fig. 4.

$$M = \begin{bmatrix} 0 & 1.07986 & 0 & 0 & 0 & 0 & 0 & 0 \\ 1.07986 & 0 & 0.88269 & 0 & 0 & 0 & 0 & 0 \\ 0 & 0.88269 & 0 & 0.60937 & 0 & 0 & 0 & 0 \\ 0 & 0 & 0.60937 & 0 & 0.55576 & 0 & 0 & 0 \\ 0 & 0 & 0 & 0.55576 & 0 & 0.60937 & 0 & 0 \\ 0 & 0 & 0 & 0 & 0.60937 & 0 & 0.88269 & 0 \\ 0 & 0 & 0 & 0 & 0 & 0.88269 & 0 & 1.07986 \\ 0 & 0 & 0 & 0 & 0 & 0 & 1.07986 & 0 \end{bmatrix} \tag{2}$$

$$M = \begin{bmatrix} 0 & -1.02981 & 0 & 0 & 0 & 0 & 0 & 0 \\ -1.02981 & 0 & 0.86421 & 0 & 0 & 0 & 0 & 0 \\ 0 & 0.86421 & 0 & 0.61898 & 0 & 0 & 0 & 0 \\ 0 & 0 & 0.61898 & 0 & -0.58946 & 0 & 0 & 0 \\ 0 & 0 & 0 & -0.58946 & 0 & 0.61898 & 0 & 0 \\ 0 & 0 & 0 & 0 & 0.61898 & 0 & -0.86421 & 0 \\ 0 & 0 & 0 & 0 & 0 & -0.86421 & 0 & 1.02585 \\ 0 & 0 & 0 & 0 & 0 & 0 & 1.02585 & 0 \end{bmatrix} \tag{3}$$

$$M = \begin{bmatrix} 0 & 1.03850 & 0 & 0 & 0 & 0 & 0 \\ 1.03850 & 0 & 0.88869 & 0 & 0 & 0 & 0 \\ 0 & 0.88869 & 0 & -0.64560 & 0 & 0 & 0 \\ 0 & 0 & -0.64560 & 0 & -0.64560 & 0 & 0 \\ 0 & 0 & 0 & -0.64560 & 0 & 0.88869 & 0 \\ 0 & 0 & 0 & 0 & 0.88869 & 0 & 1.03850 \\ 0 & 0 & 0 & 0 & 0 & 1.03850 & 0 \\ 0 & 0 & 0 & 0 & 0 & 0 & 0 \end{bmatrix} \tag{4}$$

Assuming a fixed variation of $\pm 10\%$ in all their coupling matrix coefficients, their corresponding coupling matrices values are increased and decreased by 10%. The return loss performance of the chained-function filter is plotted and compared with those of the standard Chebyshev type filters, as shown in Fig. 5. It can be observed that the chained-function filter has less significant impact on the return loss performance, for both $+10\%$ and -10% tolerance on their coupling matrices. The comparisons of the worst-case return loss performances of all the three filters are recorded, as summarized in Table 3.

It can be noted that for a 10% tolerance to the coupling coefficients, the percentage change of the 6th order chained-function filter is at 10.50%, as compared with 25.12%, and 17.31% for the 6th order

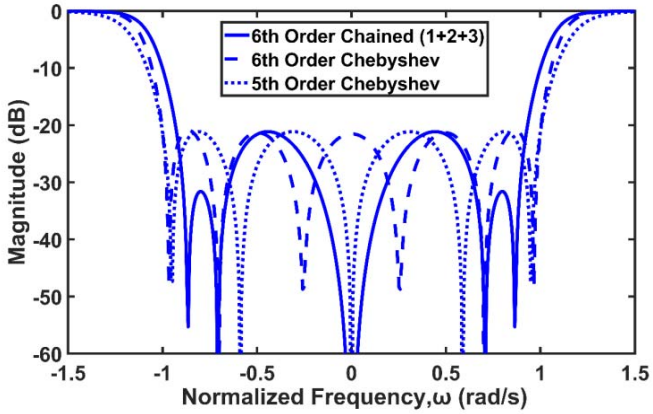

Figure 4. The theoretical lowpass prototype return loss responses of the 6th order chained-function filter and the 6th and 5th order standard Chebyshev response filters. The return loss performances are at 21.14 dB.

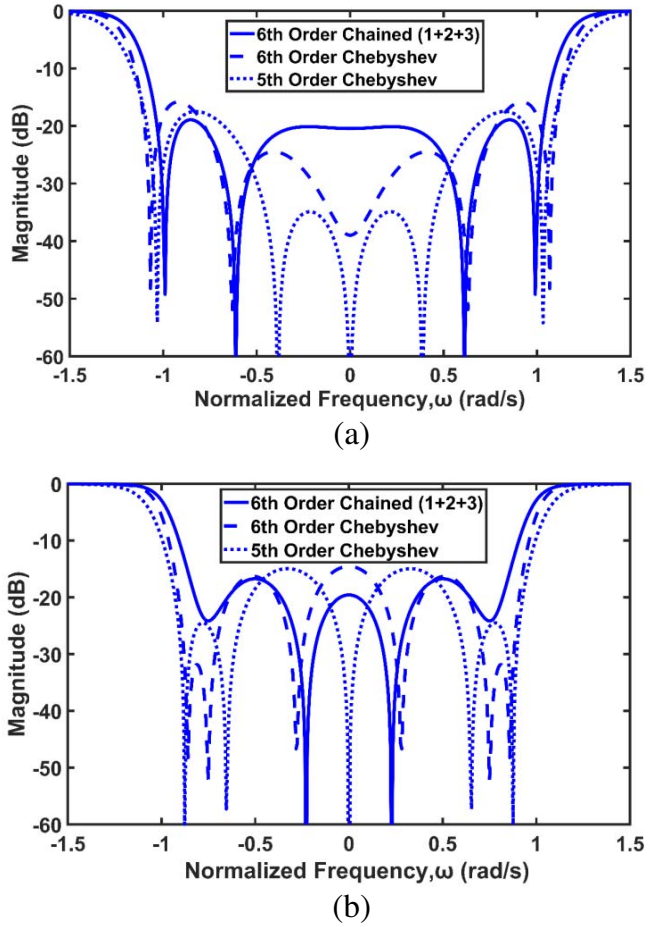

Figure 5. The effect of tolerance toward the return loss performance of the chained-function filter and the standard Chebyshev respond filters. (a) +10% tolerance, (b) −10% tolerance.

Chebyshev response filter and the 5th order Chebyshev response filter, respectively. Similarly, for a −10% tolerance to the coupling coefficients, the percentage change for the 6th order chained-function filter is at 20.86%, as compared with 31.13%, and 29.33% for the 6th order Chebyshev response filter

Table 3. Sensitivity analysis.

Category	Return Loss (dB)			Percentage Change (%)	
	Theoretical	10%	−10%	Return Loss	
				10%	−10%
6th Order Chained-Function	21.14	18.92	16.73	10.50	20.86
6th Order Chebyshev	21.14	15.83	14.56	25.12	31.13
5th Order Chebyshev	21.14	17.48	14.94	17.31	29.33

and the 5th order Chebyshev response filter, respectively. These readings suggest that the 6th order chained-function filter has a less mismatch loss, indicated by a lower percentage change of return loss performance. This clearly proves that the implementation of the chained-function concept in filter design will result in a lower sensitivity towards manufacturing error, therefore, substantially more robust than the standard Chebyshev response filter. In addition, this verifies the theoretical assumption that a wider the separation of reflection zeros leads to a lower the filter sensitivity.

As mentioned in the previous section, no chained-function filters can achieve similar (or better) out-of-band rejection properties to a standard Chebyshev response filter, given the same filter order. To achieve similar out-of-band rejection properties, one needs to increase the chained-function filter order by one. It is well known that an increase in the filter order will lead to an increase of the filter sensitivity towards manufacturing tolerance, and this claim can also be proven from the results in Table 3. It should be observed that the 6th order Chebyshev response filter has a higher percentage change for the return loss performance, for both 10% and −10% tolerance to the coupling coefficients, than those of the 5th order Chebyshev response filter. In order to have a fair comparison, the performance comparison of the 5th order Chebyshev response filter with the 6th order chained-function filter is now demonstrated.

Figure 6 shows the out-of-band rejection of the 5th order Chebyshev response filter and the 6th order chained-function filter. For the 6th order chained-function filter, we can achieve better out-of-band rejections than those of the 5th order Chebyshev response filter. In addition, based on readings in Table 3, it should be pointed out that we will still be gaining some advantages in terms of having a lower percentage changes of return-loss performance for the 6th order chained-function filter, for both 10% and −10% tolerance to the coupling coefficients, as compared with those of the 5th order Chebyshev response filter.

Therefore, one can design a chained-function filter with a slightly higher filter order but still draw a full advantage in terms of lower fabrication sensitivity to achieve the same (or better) out-of-band rejection as those of the Chebyshev response filter.

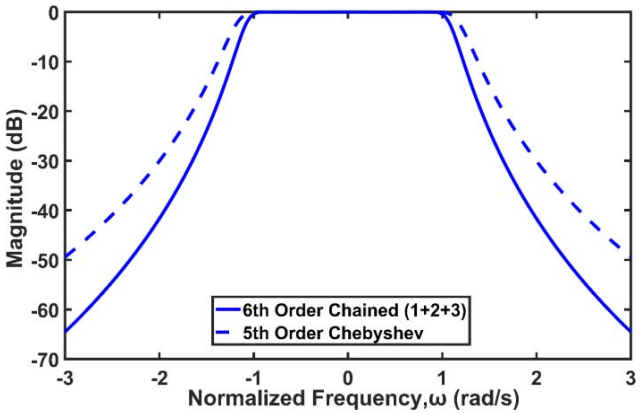

Figure 6. The out-of-band rejection slope for the 5th order Chebyshev response filter with the 6th order chained-function filter.

4. DESIGN AND SYNTHESIS

4.1. Coupling Matrix Synthesis

A 6th order chained-function polynomial, $\psi_N = 8\omega^6 - 10\omega^4 + 3\omega^2$, is formed by chaining of the prescribed lower-order generalized Chebyshev seed functions of order (1, 2, 3), as follows:

$$\psi_N = (\omega) \times \left(2\omega^2 - 1\right) \times \left(4\omega^3 - 3\omega\right) \tag{5}$$

The chained-function polynomial is used to synthesize the filter coupling matrix. The coupling matrix synthesis and similarity transformation technique (matrix rotation) [6–9] can be used to replace the classical ladder synthesis technique. This technique allows reconfiguration of the complex coupling matrix through a sequence of similarity transformations until a more convenient coupling arrangement or topology is obtained, which is physically practical for realization. Following the procedure explained in [6–9], the $N + 2$ coupling matrix, M, as depicted in Eq. (6), is formulated to represent the lowpass prototype of the filter.

$$M = \begin{bmatrix} 0 & -0.35956 & 0.48239 & -0.47018 & 0.47018 & -0.48239 & 0.35956 & 0 \\ -0.35956 & 1.21062 & 0 & 0 & 0 & 0 & 0 & 0.35956 \\ 0.48239 & 0 & 1.00926 & 0 & 0 & 0 & 0 & 0.48239 \\ -0.47018 & 0 & 0 & 0.35440 & 0 & 0 & 0 & 0.47018 \\ 0.47018 & 0 & 0 & 0 & -0.35440 & 0 & 0 & 0.47018 \\ -0.48239 & 0 & 0 & 0 & 0 & -1.00926 & 0 & 0.48239 \\ 0.35956 & 0 & 0 & 0 & 0 & 0 & -1.21062 & 0.35956 \\ 0 & 0.35956 & 0.48239 & 0.47018 & 0.47018 & 0.48239 & 0.35956 & 0 \end{bmatrix} \tag{6}$$

From the coupling matrix in Eq. (6), however, there are many unwanted cross-couplings. Thus, a reduction procedure on the coupling matrix should be carried out to produce the desired coupling matrix topology. Following the theory explained in [6–9], the in-line configuration of an $N + 2$ coupling matrix, M, is computed, as depicted in Eq. (7). The corresponding lowpass prototype network responses are plotted in Fig. 7. It should be pointed out that this technique is not limited to chained-function polynomials; therefore, other characteristics polynomials can also be adopted for this synthesis technique.

$$M = \begin{bmatrix} 0 & 1.07986 & 0 & 0 & 0 & 0 & 0 & 0 \\ 1.07986 & 0 & 0.88269 & 0 & 0 & 0 & 0 & 0 \\ 0 & 0.88269 & 0 & 0.60937 & 0 & 0 & 0 & 0 \\ 0 & 0 & 0.60937 & 0 & 0.55576 & 0 & 0 & 0 \\ 0 & 0 & 0 & 0.55576 & 0 & 0.60937 & 0 & 0 \\ 0 & 0 & 0 & 0 & 0.60937 & 0 & 0.88269 & 0 \\ 0 & 0 & 0 & 0 & 0 & 0.88269 & 0 & 1.07986 \\ 0 & 0 & 0 & 0 & 0 & 0 & 1.07986 & 0 \end{bmatrix} \tag{7}$$

From Eq. (7), it is suitable to be integrated into a wide variety of microwave technologies, such as microstrip, dielectric, coaxial, and waveguide, for application to space and terrestrial communication systems. In this paper, we integrate the coupling matrix into a waveguide technology.

4.2. Chained-Function in Waveguide

To recall, the general transfer and reflection functions of a filter can be expressed as [5]:

$$|S_{21}(\omega)|^2 = \frac{1}{1 + \varepsilon^2 \psi_N^2(\omega)} \tag{8}$$

and

$$|S_{11}(\omega)|^2 = \frac{\varepsilon^2 \psi_N^2(\omega)}{1 + \varepsilon^2 \psi_N^2(\omega)} \tag{9}$$

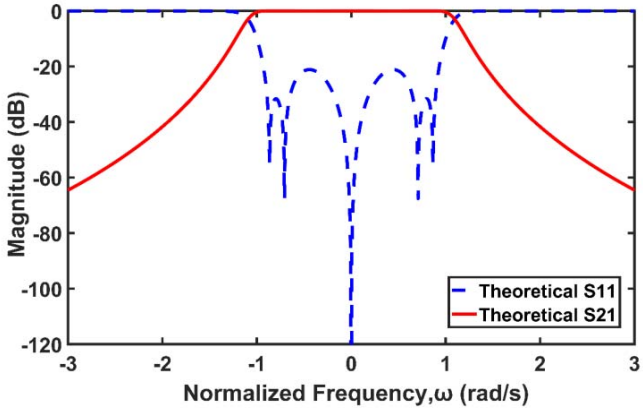

Figure 7. Transfer and reflection functions of the designed 6th order chained response filter.

where ε (having $0 < \varepsilon \leq 1$) is the ripple level in the passband, and ψ_N is known as the filtering function of N degrees. A chained-function polynomial will be adopted to act as the filtering function in this paper. For a waveguide filter, we can define ω as [5]:

$$\omega = \alpha \left(\frac{\lambda_g}{\lambda_{g0}}\right) \sin\left(\pi \frac{\lambda_{g0}}{\lambda_g}\right) \tag{10}$$

where λ_g is the guided wavelength, $\lambda_{g0} \approx (\lambda_{g1} + \lambda_{g2})/2$ where λ_{g1} and λ_{g2} are the guided wavelengths at the upper and lower band-edge frequencies, respectively; $\alpha = [(\lambda_{g1}/\lambda_{g0}) \sin(\pi\lambda_{g0}/\lambda_{g1})]^{-1}$ is the lowpass to bandpass scaling factor of a waveguide filter. Equations (8), (9), and (10) allow circuit transformation from a lowpass prototype to a waveguide bandpass filter design with arbitrary frequency, bandwidth, and specifications to fit different applications.

4.3. Prototype Design

Figure 8 shows the waveguide filter coupling diagram considered in this paper. The circles in black represent the coupled resonators, and the circles in transparent represent the input and output ports, while the solid lines represent the main line coupling.

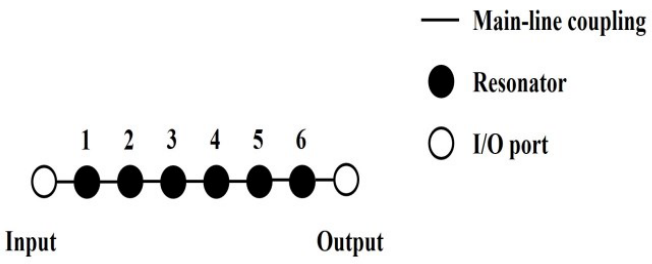

Figure 8. Coupling diagram of the waveguide filter.

The novel waveguide filter is designed to operate at 28 GHz, with a fractional bandwidth of 2% (Passband: 27.72 GHz–28.28 GHz). The lower and upper rejection properties of the filter are better than 70 dB and 65 dB at 27 GHz and 29 GHz, respectively. In addition, the in-band return loss level for the entire band of interest is better than 20 dB. Fig. 9 depicts the theoretical transfer and reflection responses of the designed waveguide filter.

These specifications can be achieved by a 6th order chained-function polynomial of order (1+2+3), with a ripple factor, ε, of 0.333. We choose a 6th order waveguide filter in order to demonstrate the

feasibility of a chained-function concept in a complex higher order narrow-band filter design. Since all the coupling coefficients in Eq. (7) are positive, the realization of the filter can be achieved based on the inductive irises rather than capacitive irises. Fig. 10 illustrates the designed configuration of the sixth order chained-function waveguide filter with its filter parameters.

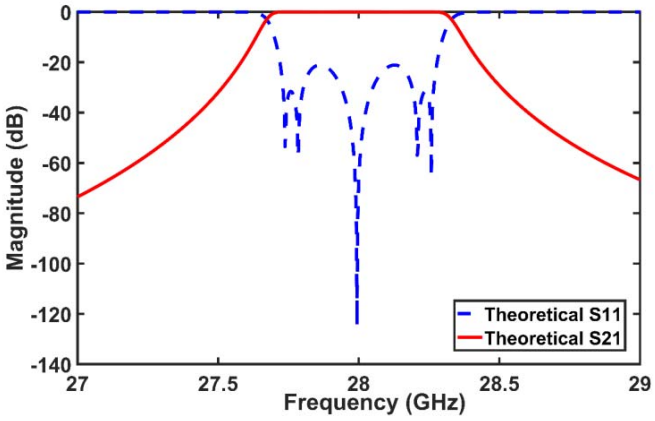

Figure 9. The transfer and reflection responses of the waveguide filter centered at 28 GHz.

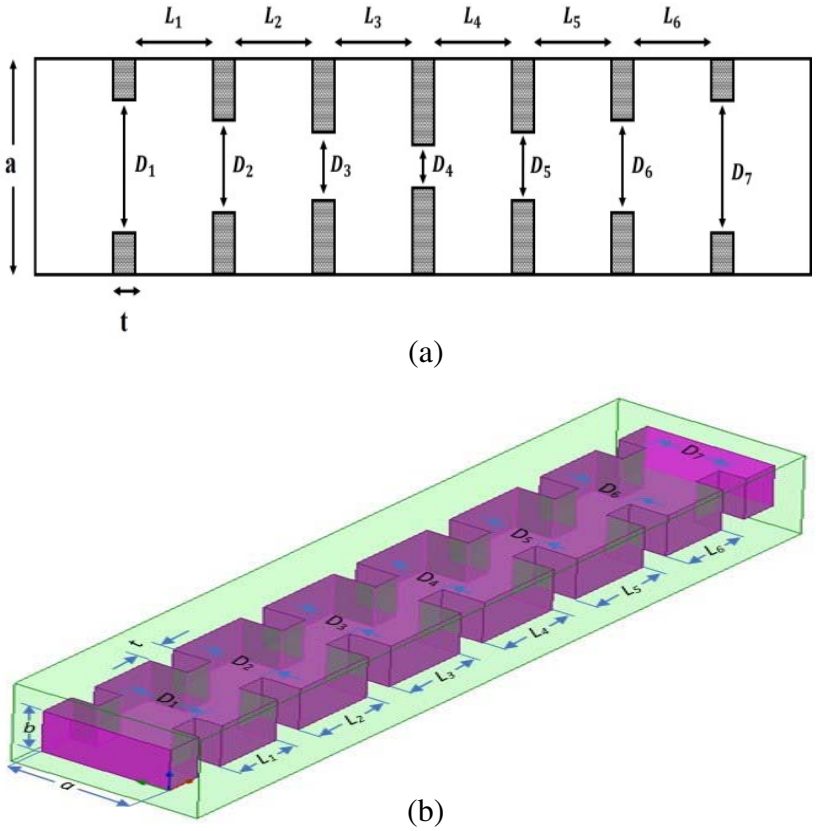

Figure 10. The 3D structure and topology of the rectangular waveguide filter and its filter design parameters. (a) Top view of the waveguide filter. (b) Geometry of the entire waveguide filter design. The final optimized filter design dimensions at 28 GHz are: $a = 8.636$ mm, $b = 4.318$ mm. Resonator length: $L_1 = L_6 = 4.895$ mm, $L_2 = L_5 = 5.835$ mm, $L_3 = L_4 = 5.975$ mm. Iris diameter: $D_1 = D_7 = 4.85$ mm, $D_2 = D_6 = 3.46$ mm, $D_3 = D_5 = 3.13$ mm, $D_4 = 3.083$ mm. Iris thickness $t = 2.359$ mm.

The six resonators waveguide filter operates at a fundamental TE_{10} mode and is designed to be symmetrical in geometry. The waveguide filter is based on the window-coupled inductive irises. It can also be observed that the filter consists of six resonators (denoted by L) and seven inductive irises (denoted by D). Since the waveguide filter operates at 28 GHz, we can use the standard WR-34 waveguide with UG-1530/U Flange, which has the cross-sectional dimensions of $a = 8.836$ mm and $b = 4.318$ mm. The initial approximations of all resonators and irises of the waveguide filter are obtained using the theory in [5, 9, 17].

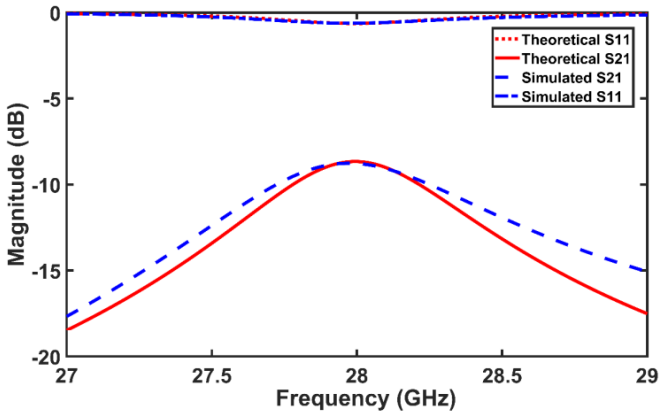

(a)

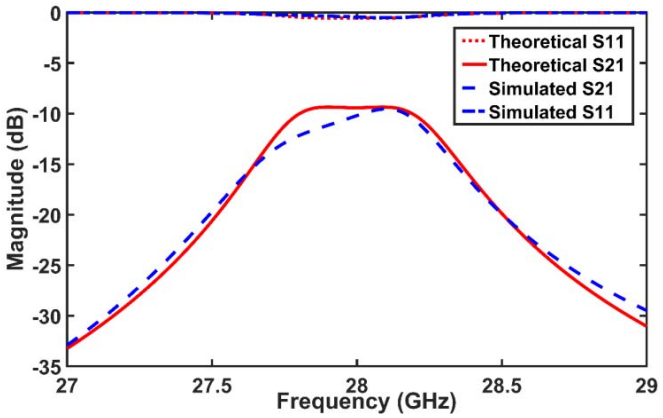

(b)

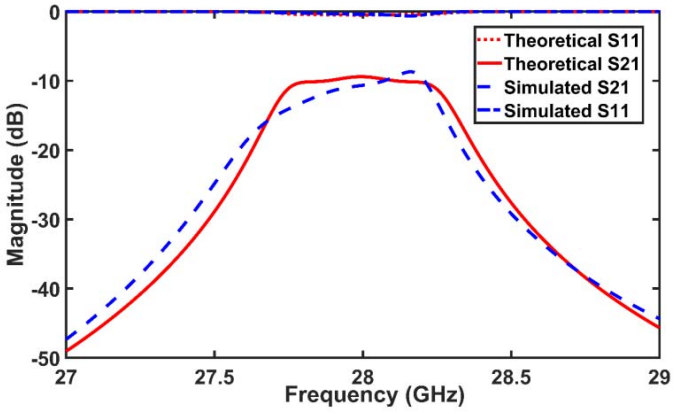

(c)

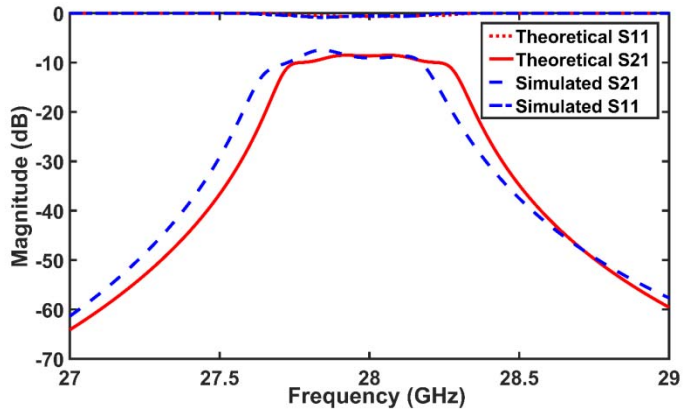

(d)

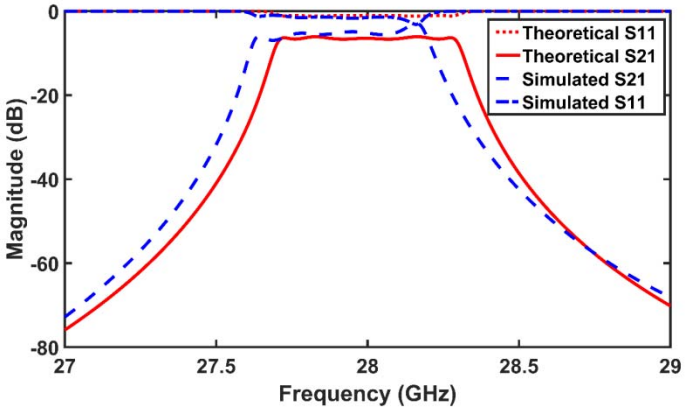

(e)

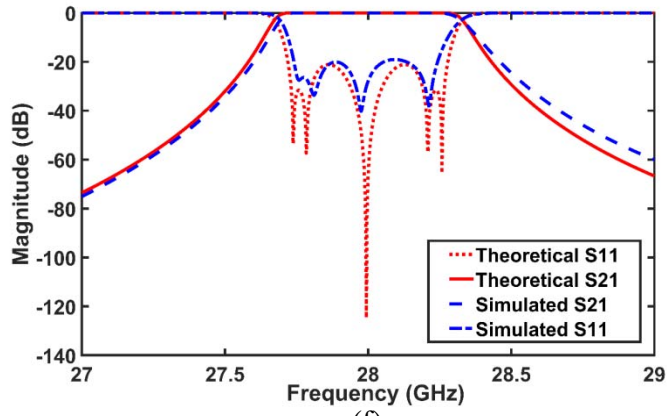

(f)

Figure 11. The simulated and theoretical S-parameter responses from step 1 to step 6, using the step-tune method.

4.4. Simulations

The simulation is carried out in ***ANSYS HFSS* (version 2013)** [18] using the step-tune method as described in [19, 20]. With the step-tune method, local optimization can be exploited to replace the complex and lengthy global optimization process. This technique significantly reduces the number of parameters to be fine-tuned, and at the same time, the simulation results are more reliable and have great convergence toward the target filter responses. Therefore, the simulation of the waveguide filter

can be divided into six sub-steps.

The waveguide filter is assigned to act as a perfect electrical conductor during the entire simulation process. In other words, the conductor loss has not been taken into consideration for the simulation. In addition, the thickness of all the irises, t, is kept constant at 2.359 mm. Instead of performing tuning and optimizing the whole waveguide structure, we simulate and optimize the waveguide structure resonator by a resonator toward a desired response.

For the first step, only one resonator and its adjacent irises are introduced into the tuning and optimization process. The coupling strength between the resonators can be controlled by tuning the diameter and the thickness of the irises, while the resonant frequency of the waveguide can be controlled by tuning the length of the resonator. After obtaining the desired responses, the simulation can be continued by adding one successive resonator at a time to the simulated structure. For this step-by-step tuning method, the key point is that the S-parameter responses for each stage can be obtained from their corresponding coupling matrices synthesized from the chained-transfer function, and be applied as the objective responses for the tuning and optimization process [19, 20].

Figures 11(a)–(f) show a comparison between the simulated and theoretical S-parameter responses of the designed chained-function waveguide filter from step 1 to step 6, respectively. Tables 4 and 5 depict the iris dimensions and resonator lengths being tuned at each successive step, respectively. The final plots of the simulated and theoretical outcomes of the waveguide filter centered at 28 GHz with 2% bandwidth and return loss of 19.59 dB and 21.14 dB, respectively, are illustrated in Fig. 11(f). In general, the two results show a good agreement.

Table 4. Iris dimensions in each successive step.

Steps	**Iris Dimensions (mm)**						
	$\mathbf{D_1}$	$\mathbf{D_2}$	$\mathbf{D_3}$	$\mathbf{D_4}$	$\mathbf{D_5}$	$\mathbf{D_6}$	$\mathbf{D_7}$
1	4.87	3.45	-	-	-	-	-
2	4.87	3.47	3.08	-	-	-	-
3	4.87	3.49	3.16	3.02	-	-	-
4	4.87	3.49	3.16	3.08	3.16	-	-
5	4.87	3.48	3.13	3.08	3.13	3.48	-
6	4.85	3.46	3.13	3.083	3.13	3.46	4.85

Table 5. Resonator length in each successive step.

Steps	**Resonator Length (mm)**					
	$\mathbf{L_1}$	$\mathbf{L_2}$	$\mathbf{L_3}$	$\mathbf{L_4}$	$\mathbf{L_5}$	$\mathbf{L_6}$
1	4.91	-	-	-	-	-
2	4.95	5.85	-	-	-	-
3	4.95	5.86	5.98	-	-	-
4	4.92	5.86	6.00	6.00	-	-
5	4.90	5.86	6.02	6.02	5.86	-
6	4.895	5.835	5.975	5.975	5.835	4.895

5. WAVEGUIDE FABRICATION

Conventional micromachining is known as the subtractive manufacturing, in which the 3D objects are constructed by successively cutting material away from a solid block of material. The subtractive manufacturing is typically accomplished with a high precision CNC milling technology. The process

involves cutting around the three axes of the 3D object. In contrast, the modern 3D printing is known as the additive manufacturing, in which the 3D objects are constructed by successively depositing materials in layers. The additive manufacturing can be shown as a rapid and relatively low-cost solution but with a lower resolution, which will result in poor surface roughness and high manufacturing errors. The chained-function waveguide filters fabricated through these two different technologies are now demonstrated.

5.1. CNC Machined Waveguide Filter

Figure 12 depicts a photograph of the final assembly waveguide filter using CNC milling process. It can be observed that the CNC machined waveguide filter is constructed into two split machined blocks to facilitate the fabrication process. The two split machined blocks are then assembled together with assembly screws and alignment pins.

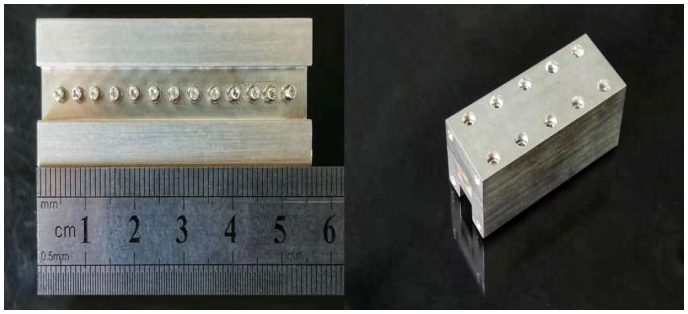

Figure 12. Photograph of the fabricated waveguide filter using CNC milling process after assembly the two split blocks. The waveguide filter is electroplated with silver.

Extra care must be taken with respect to the flatness of both machined blocks to ensure that a good electrical contact can be achieved between them. Furthermore, the screw positions and screw holes must be aligned correctly to ensure that the two halves can be fastened together. It should be noted that the radiation losses associated with the gaps between the two split blocks and screw holes are found to be insignificant through simulation in HFSS. The comparison of surface roughnesses for the waveguide filter using CNC milling and DMLS processes is presented in Fig. 14. From Fig. 14(a), the CNC machined waveguide filter exhibits a smoother surface, especially at the hollow tubing than that of the DLMS printed waveguide filter in Fig. 14(b). This is because CNC milling technology has a higher resolution. In addition, the CNC milling technology can achieve a satisfactory accuracy of $\pm 5\,\mu m$ in the physical dimension [15], in contrast to the DMLS technology which typically comes with a high manufacturing tolerance between 2 and 5 mils [21] in the physical dimension.

The CNC machined waveguide filter is machined out of Aluminum, and then the electroplating process can be employed for surface metallization. A thin layer of silver with its theoretical bulk conductivity of 6.10×10^7 (S/m) is plated on the surface of the waveguide structure, and therefore, a better attenuation performance can be achieved. At the 28 GHz operating frequency, the skin depth of silver is at $0.379\,\mu m$. To ensure sufficient coating, the waveguide filter is coated with $2\,\mu m$ thick conductive layer of silver.

5.2. DMLS Printed Waveguide Filter

Figure 13 presents a photograph of the fabricated waveguide filter using the DMLS process. Unlike the CNC machined waveguide filter, it can be observed that the waveguide filter is printed as a whole piece, and it is free from assembly, i.e., no assembly screws and/or alignment pins are needed. Therefore, the DMLS printed waveguide filter has full advantages in terms of having a more convenient integration and with less materials than those of the CNC machined waveguide filter.

The DMLS printed waveguide filter is constructed by successively depositing maraging steel power in layers by means of laser sintering. A thin layer of gold with its theoretical bulk conductivity of

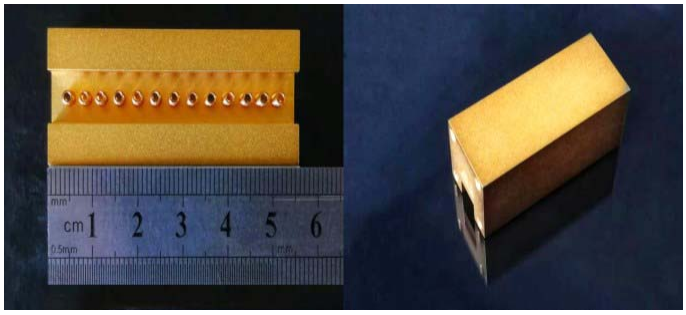

Figure 13. Photograph of the fabricated waveguide filter using DMLS printing process. The waveguide filter is electroplated with gold.

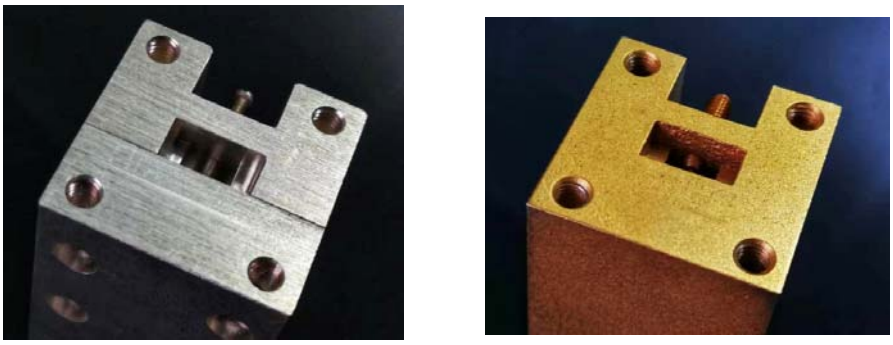

(a) (b)

Figure 14. Comparison of surface roughness for the waveguide filter using (a) CNC milling, (b) DMLS process. The CNC machined waveguide filter exhibits a smoother surface whereas the DMLS printed waveguide filter exhibits poor surface roughness. The CNC machined waveguide filter is platted with silver while the DMLS waveguide filter is platted with gold.

410×10^7 (S/m) is then plated on the surface of the waveguide using the conventional electroplating process. The gold coating layer is found to have a lower conductivity than that of silver. At the 28 GHz operating frequency, the skin depth of gold is at 0.450 µm. To ensure sufficient coating, the waveguide filter is coated with a 2 µm thick conductive layer of 24K pure gold. Due to a lower resolution, it can be noted that in Fig. 14(b), the DMLS printed waveguide filter exhibits a poor surface roughness (wrapping of the metal can be observed), as compared with that of the CNC machined waveguide filter in Fig. 14(a).

6. MEASUREMENT RESULTS

The measurements of the waveguide filters are carried out using the Agilent E8363C PNA Microwave Network Analyzer with a pair of WR-34 waveguide launchers. The PNA Network Analyzer has an operating frequency range from 10 MHz to 40 GHz. Prior to the measurement process, the network analyzer needs to be calibrated with the coaxial Short-Open-Load-Thru (SOLT) calibration to ensure accurate measurement results, using the Agilent 85056D 2.4 mm interface calibration kit. The waveguide filter is connected to the WR-34 waveguide launchers, which are connected to the network analyzer for the measurement process.

6.1. CNC Machined Waveguide Filter

Figure 15 depicts a comparison between simulated and measured performances of the CNC machined waveguide filter. As can be observed, the lower and upper rejection levels of the measured performances

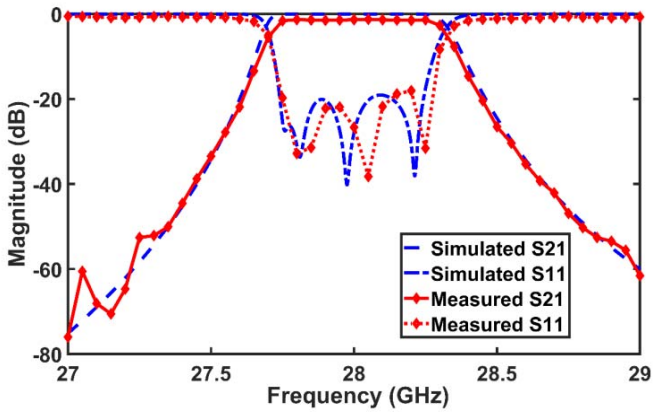

Figure 15. Comparison of simulated and measured performances of the CNC prototype waveguide filter.

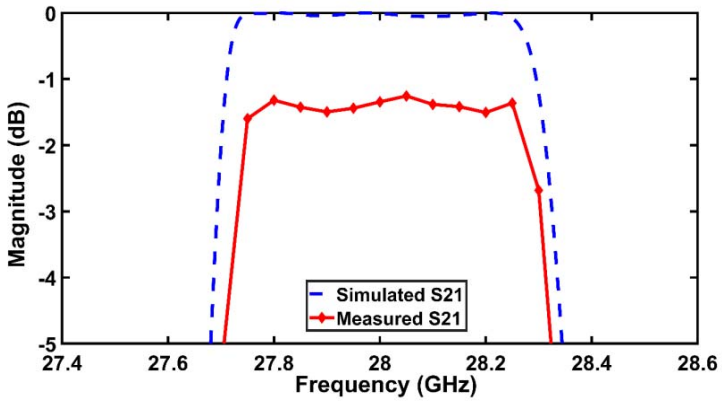

Figure 16. The expended view of the simulated and measured insertion loss level of the CNC prototype waveguide filter.

are better than 75 dB and 60 dB at 27 GHz and 29 GHz, respectively. In addition, the waveguide filter can achieve an excellent return loss performance of 18.06 dB for the entire band of interest. In Fig. 16, the expanded views of the simulated and measured performances of the filter passband insertion loss level are shown in detail. The passband insertion loss at the center frequency of 28 GHz is reported at 1.3 dB.

The simulated insertion loss of the waveguide filter using the conductivity of silver is at 0.4 dB. Obviously, the measured insertion loss is expected to be a little higher than the ideal simulated insertion loss. The difference of 0.9 dB in the passband insertion loss arises due to several factors, including: 1) The conductor loss from the waveguide launcher and the coaxial cables contributes to the additional passband insertion loss. 2) The lower worst-case return loss in the measured result than the simulated return loss. The measured performance of the waveguide filter is achieved without a complex post-manufacturing tuning process, i.e., a first pass tuning-less filter response is achieved. For this reason, it clearly indicates that the chained-function concept can be employed for designing a cost-effective yet high-performance filter. In general, all the results between simulation and measurement are in excellent agreement.

6.2. DMLS Printed Waveguide Filter

Figure 17 shows a comparison between the simulated and measured performances of the DMLS printed waveguide filter. The measured center frequency is at 27.70 GHz with the passband insertion loss at

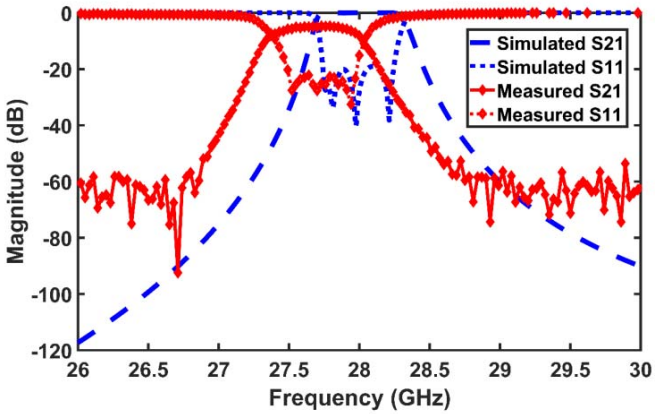

Figure 17. Comparison of simulated and measured performances of the DMLS printed waveguide filter.

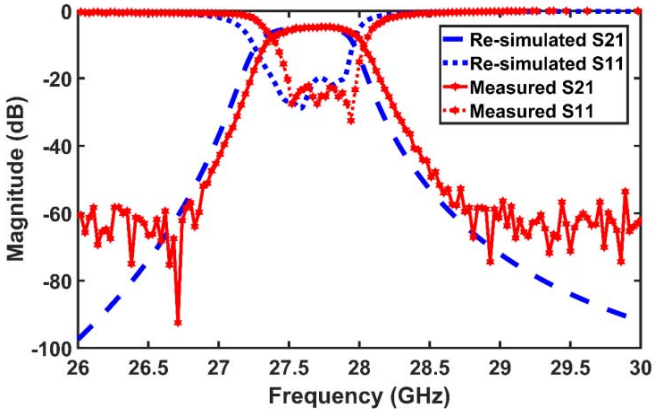

Figure 18. Comparison of re-simulated and measured performances of the DMLS printed waveguide filter.

4.95 dB. It can be observed that the waveguide filter suffers from a high passband insertion loss, and the centre frequency has been downshifted by around 300 MHz, which is just as small as 1.7%. However, the high return loss performance at 22.17 dB of the measured results clearly suggests that an excellent impedance matching between the ports is achieved.

A re-simulation model is constructed to find the root causes of the high passband insertion loss and downshifting of center-frequency. The re-simulation is conducted based on a lower bulk conductivity of of 3.00×10^5 (S/m), which is approximately 136.67 times less than the original conductivity of gold. In addition, the re-simulation model is tuned toward the center frequency of 27.70 GHz and has the same fractional bandwidth of 2% as that of the original filter specifications. The comparison of the re-simulated and measured performances are illustrated in Fig. 18, and the expanded views of their passband insertion loss levels are shown in Fig. 19. The dimensions of the irises and the resonator lengths for the original and re-simulation model of the waveguide filters are tabulated in Table 6 and Table 7, respectively.

A good agreement is achieved between the re-simulated and measured results. From Table 6 and Table 7, the average changes in percentages for the iris dimensions and resonator lengths are 6.69% and -0.46%, respectively.

Based on the re-simulation outcome, we can conclude that the high passband insertion loss of the waveguide filter fabricated through the DMLS process is mainly due to the conductor loss resulting from poor conductivity of the plating materials. It should be noted that the waveguide filter is printed as a whole piece in the DMLS process without the need of assembling; therefore, the whole waveguide

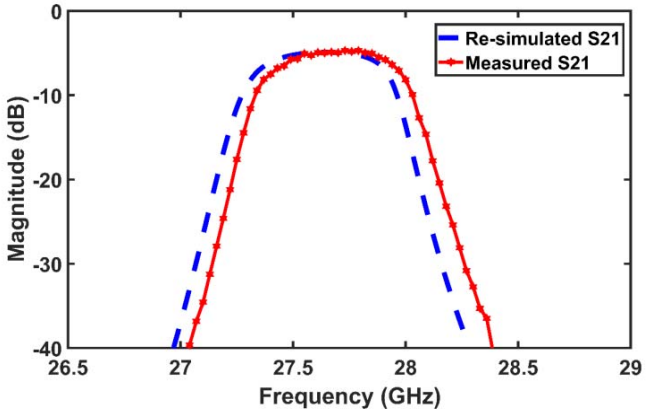

Figure 19. The expended view of the re-simulated and measured insertion loss level of the DMLS printed waveguide filter.

Table 6. The Iris dimensions for original and re-simulation.

Iris	Iris Dimensions (mm)		Percentage Change (%)	Average Percentage Change (%)
	Original	Re-simulation		
D_1	4.85	5.04	3.92	6.69
D_2	3.46	3.72	7.51	
D_3	3.13	3.39	8.31	
D_4	3.083	3.31	7.36	
D_5	3.13	3.39	8.31	
D_6	3.46	3.72	7.51	
D_7	4.85	5.04	3.92	

Table 7. The resonator lengths for original and re-simulation.

Iris	Resonator Lengths (mm)		Percentage Change (%)	Average Percentage Change (%)
	Original	Re-simulation		
L_1	4.895	4.871	−0.49	−0.46
L_2	5.835	5.800	−0.60	
L_3	5.975	5.958	−0.28	
L_4	5.975	5.958	−0.28	
L_5	5.835	5.800	−0.60	
L_6	4.895	4.871	−0.49	

structure must be immersed into the plating solution during the electroplating process. On the other hands, for the CNC machined waveguide filter, the waveguide structure can be detached and split into multiple pieces for the electroplating process. Therefore, the extremely small internal dimensions of the DMLS printed waveguide filter will have less exposure to the electroplating solution. The depletion of electroplating solution in the internal waveguide cavity will lead to uneven distribution of the current density. This may result in a lack of adhesion or coverage on the surface of waveguide cavity, therefore,

contributing to an insufficient and/or uneven metal coating layer on the surface of the finished product. This means that there will be blistering inside the waveguide cavity, and the final waveguide filter design dimensions will be inaccurate. This causes the downshifting of the waveguide center frequency and the high passband insertion loss.

With the decrease of the material conductivity, the passband insertion loss of the filter increases monotonically. Therefore, the passband insertion loss of the DMLS printed waveguide filter can be improved by following a proper electroplating process to achieve a uniform coat for the entire structure. The only way to overcome this problem is by employing a split-block method, in which the waveguide filter is split into multiple blocks for fabrication, in order to give an acceptable metal plating so that the error in dimensions of the finished product is minimized.

7. CONCLUSION AND RECOMMENDATIONS

In this paper, we have presented the evaluation of a chained-function to design a waveguide filter at 28 GHz for millimeter-wave applications. Two manufacturing technologies, namely the CNC machining and DMLS printing, are utilized as the potential fabrication methods. The reduced sensitivity of the filter has been theoretically and practically demonstrated using a window-coupled inductive iris rectangular waveguide structure. In other words, the theoretical, simulated, and measured results are in good agreement in both CNC machined and DMLS printed waveguide filters, if the effect of conductivity is taken into account in the simulation model for the DMLS printed waveguide filter. The simulation outcomes indicate that the main loss of the DMLS printed filter is mainly due to the conductor loss resulting from uneven and/or insufficient plating. The chained-functions, which lie in between the Butterworth and Chebyshev approximations, can bridge between the lower fabrication sensitivity and lower loss responses of Butterworth approximation, while maintaining an excellent out-of-band rejection performance comparable with that of the conventional Chebyshev approximation for the same filter order.

While the chained-function concept in filter design looks promising for rapid prototyping due to the properties of reduced sensitivity to manufacturing tolerance, there are still many rooms for improvements, especially for the manufacturing and surface metallization processes. Therefore, for further work, a polymer-based 3D printed waveguide filter can be investigated. The waveguide filter can be manufactured by a polymer jetting (polyjet) additive manufacturing technology. Then, a proper surface metallization process can be employed to provide a better attenuation performance. Clearly, the polymer-based 3D printed waveguide filter will draw full benefits in terms of having low-mass and low production cost, as compared with those of the waveguide filter realized by solid metal. In summary, the chained-function concept based on the partition theory can be exploited as an attractive alternative to a rapid, low-cost, high-performance, and sustainable filter design, especially at the higher millimeter-wave band.

ACKNOWLEDGMENT

The authors acknowledge YUTP (015LC0-106) and PRGS (0153AB-L50) for the funding support. The authors would like to thank Jason Joo and Paulene Siew, from Additive 3D Asia for the fabrication of the waveguide filter.

REFERENCES

1. Chrisostomidis, C. E. and S. Lucyszyn, "Seed function combination selection for chained function filters," *IET Microwaves, Antennas Propag.*, Vol. 4, No. 6, 799–807, 2010.
2. Chrisostomidis, C. E. and S. Lucyszyn, "On the theory of chained-function filters," *IEEE Trans. Microw. Theory Tech.*, Vol. 53, No. 10, 3142–3151, 2005.
3. Guglielmi, M. and G. Connor, "Chained function filters," *IEEE Microw. Guid. Wave Lett.*, Vol. 7, No. 12, 390–392, 1997.

4. Chrisostomidis, C. E., M. Guglielmi, P. Young, and S. Lucyszyn, "Application of chained functions to low-cost microwave band-pass filters using standard PCB etching techniques," *2000 30th European Microwave Conference*, 1–4, 2000.
5. Hunter, I., *Theory and Design of Microwave Filters*, 368 pages, The Institution of Engineering and Technology, 2001.
6. Cameron, R. J., "General coupling matrix synthesis methods for Chebyshev filtering functions," *IEEE Trans. Microw. Theory Tech.*, Vol. 47, No. 4, 433–442, 1999.
7. Lim, Y. P., Y. L. Toh, S. Cheab, S. Lucyszyn, and P. W. Wong, "Coupling matrix synthesis and design of a chained-function waveguide filter," *2018 Asia-Pacific Microwave Conference (APMC)*, 103–105, 2018.
8. Cameron, R. J., "Advanced coupling matrix synthesis techniques for microwave filters," *IEEE Trans. Microw. Theory Tech.*, Vol. 51, No. 1, 1–10, 2003.
9. Cameron, R. J., C. M. Kudsia, and R. R. Mansour, *Microwave Filters for Communication Systems*, Chapters 1–30, Wiley-Interscience, 2018.
10. Muller, A. A., J. Favennec, and E. Sanabria-Codesal, "Coupling matrix filter synthesis based on reflection matrices," *2015 Asia-Pacific Microwave Conference (APMC)*, Vol. 1, 1–3, 2015.
11. Muller, A. A., A. Moldoveanu, V. Asavei, E. Sanabria-Codesal, and J. F. Favennec, "Lossy coupling matrix filter synthesis based on hyperbolic reflections," *2016 IEEE MTT-S International Microwave Symposium (IMS)*, 1–4, 2016.
12. Leal-Sevillano, C. A., J. R. Montejo-Garai, J. A. Ruiz-Cruz, and J. M. Rebollar, "Low-loss elliptical response filter at 100 GHz," *IEEE Microw. Wirel. Components Lett.*, Vol. 22, No. 9, 459–461, 2012.
13. Liao, X., L. Wan, Y. Yin, and Y. Zhang, "W-band low-loss bandpass filter using rectangular resonant cavities," *IET Microwaves, Antennas Propag.*, Vol. 8, No. 15, 1440–1444, 2014.
14. Leal-Sevillano, C. A., T. J. Reck, G. Chattopadhyay, J. A. Ruiz-Cruz, J. R. Montejo-Garai, and J. M. Rebollar, "Development of a wideband compact orthomode transducer for the 180–270 GHz band," *IEEE Trans. Terahertz Sci. Technol.*, Vol. 4, No. 5, 634–636, 2014.
15. Zhuang, J.-X., W. Hong, and Z.-C. Hao, "Design and analysis of a terahertz bandpass filter," *2015 IEEE International Wireless Symposium (IWS 2015)*, 1–4, 2015.
16. Shang, X., et al., "W-band waveguide filters fabricated by laser micromachining and 3-D printing," *IEEE Trans. Microw. Theory Tech.*, Vol. 64, No. 8, 2572–2580, 2016.
17. Vanin, F. M., D. Schmitt, and R. Levy, "Dimensional synthesis for wide-band waveguide filters and diplexers," *IEEE Trans. Microw. Theory Tech.*, Vol. 52, No. 11, 2488–2495, 2004.
18. "ANSOFT HFSS," ANSYS Electromagnetic Suite 18.0, SAS IP, Inc., US, 2013.
19. Damou, M., K. Nouri, M. Feham, and M. Chetioui, "Design and optimization of rectangular waveguide filter based on direct coupled resonators," *Int. J. Electron. Telecommun.*, Vol. 63, No. 4, 375–380, 2017.
20. Shang, X., W. Xia, and M. J. Lancaster, "The design of waveguide filters based on cross-coupled resonators," *Microwave and Optical Technology Letters*, Vol. 56, No. 1, 3–8, 2014.
21. Chieh, J. S., M. Civerolo, and A. Clawson, "A ultra wideband radial combiner for X/Ku-band using CNC and DMLS processes," *IEEE Microw. Wirel. Components Lett.*, Vol. 25, No. 5, 286–288, 2015.